Linking Large-Scale Double-ITCZ Bias to Local-Scale Drizzling Bias in Climate Models

WENYU ZHOU,[a] L. RUBY LEUNG,[a] AND JIAN LU[a]

[a] *Pacific Northwest National Laboratory, Richland, Washington*

(Manuscript received 10 May 2022, in final form 8 August 2022)

ABSTRACT: Tropical precipitation in climate models presents significant biases in both the large-scale pattern (i.e., double intertropical convergence zone bias) and local-scale characteristics (i.e., drizzling bias with too frequent drizzle/convection and reduced occurrences of no and heavy precipitation). By untangling the coupled system and analyzing the biases in precipitation, cloud, and radiation, this study shows that local-scale drizzling bias in atmospheric models can lead to large-scale double-ITCZ bias in coupled models by inducing convective-regime-dependent biases in precipitation and cloud radiative effects (CRE). The double-ITCZ bias consists of a hemispherically asymmetric component that arises from the asymmetric SST bias and a nearly symmetric component that exists in atmospheric models without the SST bias. By increasing light rain but reducing heavy rain, local-scale drizzling bias induces positive (negative) precipitation bias in the moderate (strong) convective regime, leading to the nearly symmetric wet bias in atmospheric models. By affecting the cloud profile, local-scale drizzling bias induces positive (negative) CRE bias in the stratocumulus (convective) regime in atmospheric models. Because the stratocumulus (convective) region is climatologically more pronounced in the southern (northern) tropics, the CRE bias is deemed to be hemispherically asymmetric and drives warm and wet (cold and dry) biases in the southern (northern) tropics when coupled to ocean. Our results suggest that correcting local-scale drizzling bias is critical for fixing large-scale double-ITCZ bias. The drizzling and double-ITCZ biases are not alleviated in models with mesoscale (0.25°–0.5°) or even storm-resolving (~3 km) resolution, implying that either large-eddy simulation or fundamental improvement in small-scale subgrid parameterizations is needed.

KEYWORDS: Precipitation; Climate models; Clouds; Model evaluation/performance; Parameterization

1. Introduction

Global climate models (GCMs) are our major tool to understand and predict the complex climate system, yet they suffer from systematic biases in their simulations of tropical precipitation, reducing our confidence in their modeling of water cycle variability and change. One outstanding precipitation bias is the so-called double intertropical convergence zone (double-ITCZ) bias (e.g., Mechoso et al. 1995; Lin 2007; Li and Xie 2014). In contrast to observations that feature a dominant ITCZ in the northern tropics (except in spring when the ITCZ is briefly present in the southern tropical Pacific), GCMs simulate excessive precipitation in the southern tropics and pronounced ITCZs in both hemispheres. Despite generations of model development, the double-ITCZ bias has persisted (e.g., Fiedler et al. 2020; Tian and Dong 2020), impairing not only the simulation of tropical climate and variability but also the representation of the tropical–extratropical interactions (Zhou and Xie 2015; Dong et al. 2021). Therefore, it is of great importance to understand and correct the double-ITCZ bias.

The causes of the double-ITCZ bias have long been studied and our understanding has evolved over the past decades. Pioneering studies have attributed the double-ITCZ bias to underestimated surface wind stress and overestimated shortwave radiation in the southeastern tropical Pacific Ocean that induce warm SST bias and consequently anomalous precipitation (e.g., Ma et al. 1996; de Szoeke and Xie 2008). It was later argued that tropical precipitation may be influenced remotely by extratropical biases through energetic constraint (e.g., Hwang and Frierson 2013). In particular, climate models tend to simulate too few clouds and consequently too much incoming shortwave radiation in the Southern Ocean (e.g., Trenberth and Fasullo 2010). To balance this remote anomalous energy input, anomalous northward cross-equatorial energy transport may be excited in the atmosphere (Kang et al. 2008), leading to cross-equatorial circulation with enhanced (reduced) precipitation in the southern (northern) tropics. However, a few follow-up studies showed that the anomalous energy input in the Southern Ocean can be instead compensated by ocean energy transport (Hawcroft et al. 2017; Kay et al. 2012; Tomas et al. 2016), middle latitudinal processes (Adam et al. 2018), or tropical transient eddies (Xiang et al. 2018), so it only has marginal impacts on tropical precipitation. Furthermore, by untangling the coupled system, recent studies found that tropical radiative bias in atmospheric models is responsible for the hemispherically asymmetric tropical SST and precipitation biases (e.g., Xiang et al. 2017; Zhou and Xie 2017b). These studies reaffirm the importance of tropical radiation bias, but it remains unclear what processes drive tropical radiation bias and why tropical radiation bias is hemispherically asymmetric (inducing warm and wet biases in the southern tropics but cold and dry bias in the northern

Supplemental information related to this paper is available at the Journals Online website: https://doi.org/10.1175/JCLI-D-22-0336.s1.

Corresponding author: Wenyu Zhou, wenyu.zhou@pnnl.gov

DOI: 10.1175/JCLI-D-22-0336.1

TABLE 1. Names and output availability (× means the output is available) of the 16 CMIP5 and 19 CMIP6 models used in this study.

	Model name	CMIP experiment (coupled to dynamic ocean)	AMIP experiment (forced with observed SST)	Daily precipitation output	*CALIPSO* simulator cloud output
CMIP5 (1979–2008)	ACCESS1-3			×	
	BCC-CSM1-1				
	BNU-ESM			×	
	CanESM2			×	×
	CCSM4			×	
	CESM1-CAM5			×	×
	CNRM-CM5			×	×
	GFDL-CM3			×	×
	GISS-E2-R				
	HadGEM2-ES			×	×
	IPSL-CM5A-LR			×	×
	INM-CM4			×	
	MIROC5			×	×
	MPI-ESM-LR			×	×
	MRI-CGCM3			×	
	NorESM1-M	×	×	×	
CMIP6 (1979–2014)	ACCESS-CM2			×	
	BCC-CSM2-MR			×	×
	CAMS-CSM1			×	
	CESM2			×	×
	CMCC-CM2-SR5			×	
	CNRM-CM6			×	×
	CanESM5			×	×
	E3SM			×	×
	GFDL-CM4			×	×
	GISS-E2-1-G				
	HadGEM3-GC31-LL			×	
	INM-CM5			×	
	IPSL-CM6A-LR			×	×
	KACE-1-0-G			×	
	MIROC6			×	×
	MPI-ESM1-2-LR			×	
	MRI-ESM2			×	×
	NESM3			×	
	NorESM2-LM			×	

tropics). Also, previous studies have mainly focused on the hemispherically asymmetric precipitation bias linked to the SST bias, while much less attention has been paid to the precipitation bias that exists in models even without the SST bias.

Besides large-scale double-ITCZ bias, GCMs also present fundamental errors in representing local-scale precipitation characteristics such as the probability density distribution of precipitation rate. Compared to observations that feature intermittent periods of precipitation and no precipitation, GCMs simulate too infrequent periods of no precipitation, too frequent drizzle and light precipitation, and too little heavy precipitation (Dai 2006; Stephens et al. 2010; Trenberth and Zhang 2018; Fiedler et al. 2020). These model biases in local-scale precipitation characteristics are often referred to as "the drizzling bias," which is expected to influence cloud formation and consequently affect the cloud radiative effect (Bodas-Salcedo et al. 2011; Zhang et al. 2005; Nam et al. 2012; Kay et al. 2012). Given its potential impacts on mean precipitation and cloud radiative effect (CRE), local-scale drizzling bias may contribute to large-scale double-ITCZ bias. However, such a potential link has not been investigated in previous studies, which mostly studied the local- and large-scale biases separately.

This study aims to elucidate a physical link from local-scale drizzling bias to large-scale double-ITCZ bias. Section 2 describes the observation datasets and model outputs used in this study. Section 3 illustrates the atmospheric origin of the double-ITCZ bias. The double-ITCZ bias in coupled models is decomposed into a hemispherically symmetric component that exists already in atmospheric models without the SST bias and a hemispherically asymmetric component that arises from the asymmetric SST bias forced by tropical CRE bias in atmospheric models. Section 4 elucidates the dependencies of tropical CRE and precipitation biases in atmospheric models on the climatological convective regime and how the dependencies lead to symmetric precipitation bias but asymmetric CRE bias. Section 5 illustrates how local-scale drizzling bias leads to convective-regime-dependent biases in precipitation

TABLE 2. List of the seven models in HighResMIP that provide paired AMIP-style simulations of high (mesoscale resolution at 0.25°–0.5°, referred to as HiRes) and low (standard resolution at 1°–2°, referred to as LoRes) horizontal resolutions.

	Model name (atmosphere resolution)		Model name (atmosphere resolution)
HiRes (mesoscale resolution)	CNRM-CM6-1-HR (~0.5°)	LoRES (standard resolution)	CNRM-CM6-1 (~1°)
	GFDL-CM4-C192 (~0.47°)		GFDL-CM4 (~1°)
	HadGEM3-GC31-HR (~0.5°)		HadGEM3-GC31-LR (~1.35°)
	INM-CM5-H (0.67° × 0.5°)		INM-CM5 (~1.4°)
	IPSL-CM6A-ATM-HR (0.7° × 0.5°)		IPSL-CM6A-LR (~1.6°)
	MPI-ESM1-2-XR (~0.5°)		MPI-ESM1-2-LR (~2°)
	MRI-AGCM3-2-S (~0.25°)		MRI-ESM2 (~1°)

and CRE. Section 6 shows that these local- and large-scale precipitation biases persist in models with mesoscale and storm-resolving horizontal resolutions. Overall, our results establish a physical (direct + SST-mediated) pathway from local-scale drizzling bias to large-scale double-ITCZ bias. Section 7 provides a summary and discusses the implications.

2. Datasets and methods

a. Observations

Daily and monthly precipitation is obtained from multiple datasets, including GPCP (Global Precipitation Climatology Project; Adler et al. 2018), TRMM (Tropical Rainfall Measuring Mission; Huffman et al. 2007), CMORPH (Climate Prediction Center Morphing; Joyce et al. 2004), and PERSIANN-CDR (Precipitation Estimation from Remotely Sensed Information using Artificial Neural Networks–Climate Data Record; Ashouri et al. 2015). Monthly SSTs are obtained from the Hadley Centre Sea Ice and Sea Surface Temperature (HadISST) dataset (Rayner et al. 2003). Monthly cloud fraction is obtained from the GCM Oriented Cloud *CALIPSO* (*Cloud–Aerosol Lidar and Infrared Pathfinder Satellite Observations*) Product (Chepfer et al. 2010). Monthly radiative fluxes at the top of the atmosphere (TOA) are obtained from the Clouds and the Earth's Radiant Energy System (CERES) dataset (Wielicki et al. 1996). The SST dataset covers the period of 1979–2014. The *CALIPSO* cloud fraction dataset covers the period of 2006–14. The CERES radiation dataset covers the period of 2001–14. The precipitation datasets cover the period of 1979–2014 for GPCP and TRMM and the period of 1998–2008 for CMORPH and PERSIANN-CDR. The model biases are much larger than decadal variability in observations and thus robust to exact periods chosen for analysis.

b. AMIP and CMIP

Tropical precipitation bias in coupled climate models can be decomposed into two parts—the part that exists in atmospheric models without the SST bias and the part that arises from the SST bias in coupled models. The first part is measured as the difference between observations and the Atmospheric Model Intercomparison Project (AMIP) simulations (i.e., atmosphere–land simulations forced with observed SST). The second part is measured as the difference between AMIP and Coupled Model Intercomparison Project (CMIP; historical simulations with a fully coupled ocean). Outputs of daily and monthly precipitation, monthly *CALIPSO*-simulator cloud fraction, monthly radiative fluxes, and monthly SST have been obtained from 16 models in CMIP5 (Taylor et al. 2011) and 19 models in CMIP6 (Eyring et al. 2016) that provide paired AMIP and CMIP simulations (Table 1).

c. HighResMIP

The High Resolution Model Intercomparison Project (HighResMIP) provides paired AMIP-style simulations over 1979–2014 with standard (1°–2°) and enhanced (0.25°–0.5°) horizontal resolutions (Haarsma et al. 2016). Here, paired simulations of seven models (Table 2) are compared to assess the impact of enhanced horizontal resolutions on tropical precipitation biases. The simulations with enhanced, mesoscale horizontal resolution are referred to as HiRes and the simulations with low, standard horizontal resolution are referred to as LoRes.

d. DYAMOND

The Dynamics of the Atmospheric General Circulation Modeled on Nonhydrostatic Domains (DYAMOND) project is the first intercomparison project of global storm-resolving

TABLE 3. The five DYAMOND models used in this study, with references and information on the use of shallow convection parameterization. More details about these models can be found in Stevens et al. (2019).

	Model name	References	Shallow convection
DYAMOND (nonhydrostatic storm-resolving model)	FV3-3.25km	Lin (2004)	Not used
	GEOS-3km	Putman and Suarez (2011)	A nonprecipitating scheme by use of a stochastic Tokioka constraint
	NICAM-3km	Satoh et al. (2014)	Not used
	SAM-4km	Khairoutdinov et al. (2022)	Not used
	UM-5km	Wood et al. (2014), Walters et al. (2019)	A closure based on Grant (2001)

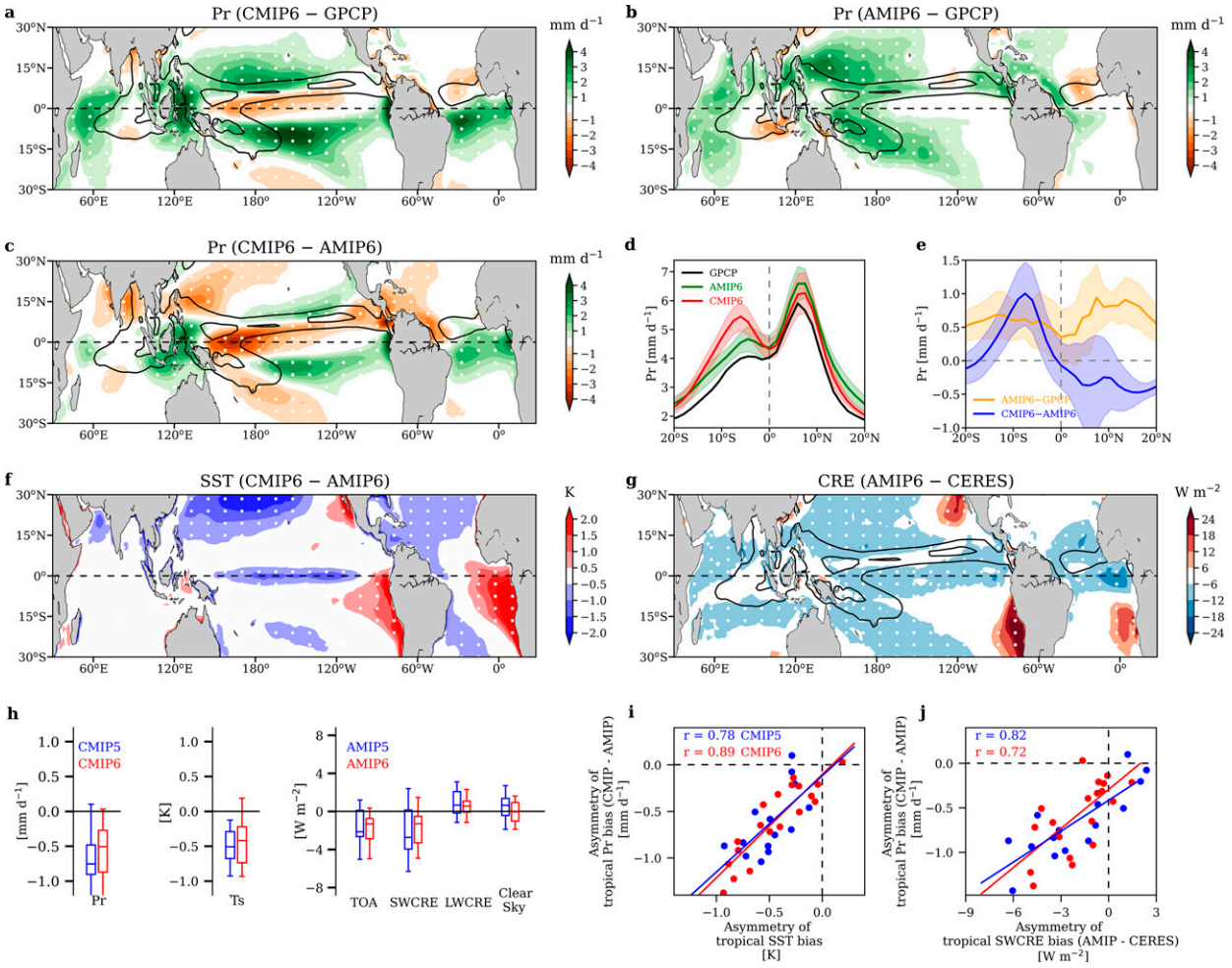

FIG. 1. (a) Spatial pattern of annual-mean tropical precipitation bias in CMIP simulations (CMIP6 − GPCP), and decomposition into (b) the part that exists in AMIP simulations without the SST bias (AMIP6 − GPCP) and (c) the part that arises from the SST bias after coupling to ocean (CMIP6 − AMIP6). The black contours indicate the annual-mean precipitation climatology (drawn at 5, 8, and 11 mm day^{-1}). (d) Annual-mean zonal-mean precipitation in GPCP, AMIP6 and CMIP6. (e) Annual-mean zonal-mean precipitation bias that exists without the SST bias (orange) and that arises after coupling to ocean (blue). (f) Spatial pattern of annual-mean tropical SST bias (CMIP6 − AMIP6). (g) Spatial pattern of annual-mean tropical CRE (TOA; downward is positive) bias in AMIP simulations (AMIP6 − CERES). (h) Boxplots of the hemispheric asymmetry of tropical precipitation and SST biases arising after coupling (CMIP − AMIP) and of tropic TOA radiation bias (decomposed into SWCRE, LWCRE, and clear-sky) that exists in AMIP simulations without the SST bias (AMIP − CERES). The box indicates the lower and upper quantiles while the whiskers indicate the range of data. (i) Scatterplot between hemispheric symmetry of tropical SST and precipitation biases arising after coupling (CMIP − AMIP). (j) Scatterplot between hemispheric symmetry of tropical SWCRE bias in AMIP simulations without the SST bias (AMIP − CERES) and hemispheric symmetry of tropical precipitation bias that arises from the SST bias after coupling (CMIP − AMIP). Both the CMIP5 (blue) and CMIP6 (red) results are shown in (h)–(j). The white stippling in maps indicates where more than 75% of the models agree on the sign of the changes.

simulations (Stevens et al. 2019). The atmospheric models are nonhydrostatic and use a storm-resolving (also referred to as cloud-resolving) horizontal resolution of a few kilometers. Due to the tremendous computational resources needed for such storm-resolving resolutions, model simulations only span a short 40-day period from 1 August to 10 September 2016, with prescribed observed initial and boundary conditions. Daily precipitation is obtained from five models (Table 3) whose outputs are available and compared with observations for the period of 11 August–10 September 2016.

e. *Metrics and definitions*

The hemispheric asymmetry of tropical precipitation, SST, or CRE is computed as $\vartheta_{\text{Asym}} = \overline{\vartheta}_{0\text{–}30^\circ\text{N}} - \overline{\vartheta}_{0\text{–}30^\circ\text{S}}$, where $\overline{\vartheta}$ refers to the monthly or annual mean precipitation, SST, or CRE over all the ocean grid points within the specified latitudinal range. The hemispheric asymmetry of the area of a specific convective regime is computed as $A_{\text{Asym}} = A_{0\text{–}30^\circ\text{N}} - A_{0\text{–}30^\circ\text{S}}$, where A refers to the total area of the regime of stratocumulus, moderate convection, or strong convection over the ocean

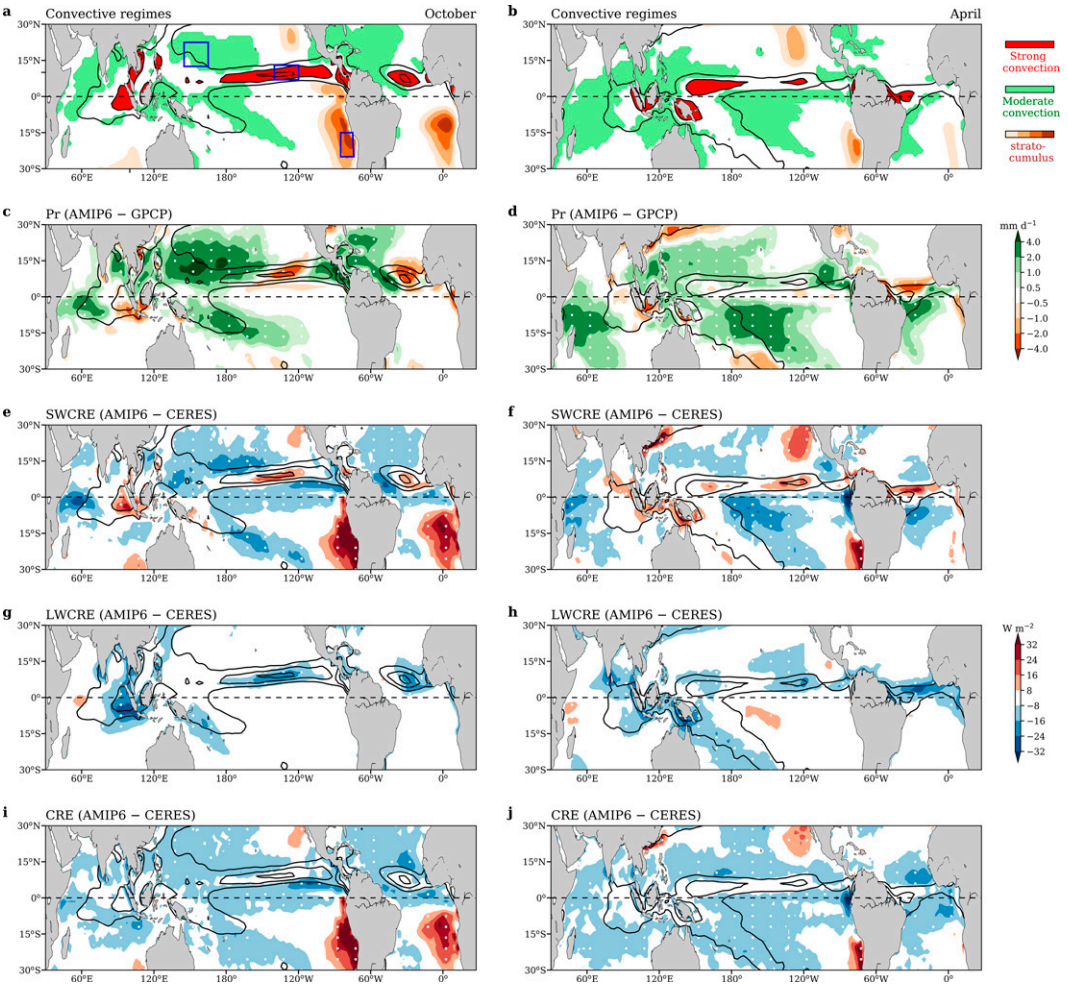

FIG. 2. (a),(b) Spatial pattern of convective regimes of stratocumulus (LLC $>$ 0.5), moderate convection ($1.5 < \overline{P} < 6$ mm day^{-1} and LCC $<$ 0.25) and strong convection ($\overline{P} > 8$ mm day^{-1}) in observations for October and April, respectively. The three representative regions used in Fig. 4 are denoted by the blue rectangles in (a). (c),(d) Spatial pattern of tropical precipitation bias in AMIP simulations (AMIP6 − GPCP) in October and April, respectively. (e)–(j) As in (c) and (d), but for the biases of the shortwave cloud radiative effect (SWCRE), longwave cloud radiative effect (LWCRE), and net cloud radiative effect (CRE). Black contours indicate the monthly precipitation climatology (drawn at 5, 8, and 11 mm day^{-1}). The white stippling indicate where more than 75% of the models agree on the sign of the changes.

within the specified latitudinal range. The regime of strong convection is defined by monthly precipitation $\overline{P} > 8$ mm day^{-1}; the stratocumulus regime is defined by monthly low-level cloud fraction (LLC) $>$ 0.5; the regime of moderate convection sits in between and is defined by $1.5 < \overline{P} < 6$ mm day^{-1} and LLC $<$ 0.25.

All the observation and model data have been interpolated to a common grid of $1° \times 1°$ before analyses and comparison.

3. Atmospheric origins of tropical precipitation bias in coupled models

The large-scale bias of tropical precipitation in coupled models depicts the well-known double-ITCZ bias, with dry bias in the equatorial Pacific Ocean and wet bias on both sides of the equator but more pronounced in the southern tropics (Fig. 1a; CMIP6 − GPCP). This double-ITCZ bias can be decomposed into the part that exists in AMIP models without the SST bias (Fig. 1b; AMIP6 − GPCP) and the part that arises from the SST bias after coupling AMIP models to ocean (Fig. 1c; CMIP6 − AMIP6). The precipitation bias in AMIP models features dry bias in regions of strong climatological convection (i.e., the Maritime Continent and the centers of the ITCZs over the eastern Pacific and Atlantic Oceans) and wet bias over surrounding regions of climatologically moderate convection (Fig. 1b). In the zonal mean, this leads to a nearly hemispherically symmetric wet bias on both the northern and southern flanks of the equator (green line vs black line in Fig. 1d; orange line in Fig. 1e). The precipitation bias that arises from the SST bias, on the other hand, features

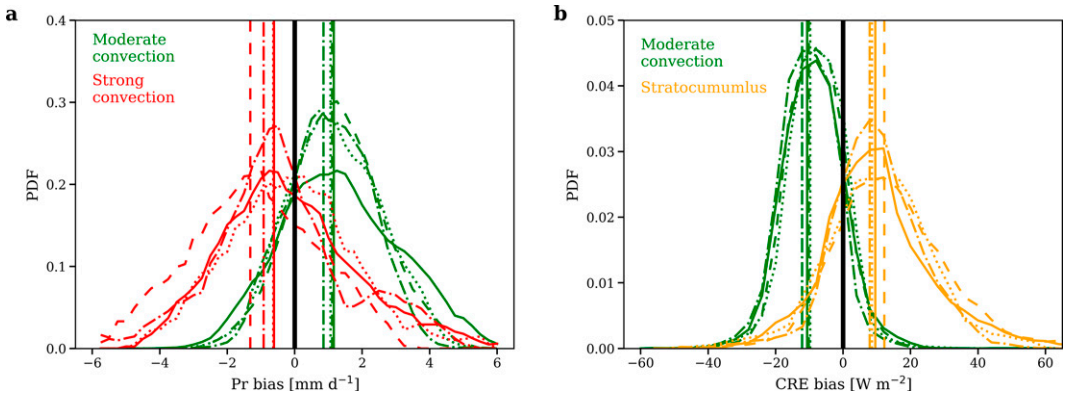

FIG. 3. (a) Distributions of the precipitation bias over the regimes of moderate (green) and strong convection in AMIP simulations (red). (b) As in (a), but for distributions of the CRE bias over the regime of moderate convection (green) and stratocumulus (orange). The PDF is constructed from the monthly biases over all grid points within individual convective regimes. The dash-dotted, dotted, solid, and dashed lines indicate the results of February, May, August, and November, respectively. The vertical line indicate the mean of all the grid points over the specific regime.

wet bias over the southern tropical Pacific and Atlantic but dry bias over the northwestern Pacific and Atlantic (Fig. 1c). In the zonal mean, this leads to an asymmetric precipitation bias that wets the southern tropics but dries the northern tropics (red line vs green line in Fig. 1d, blue line in Fig. 1e). In combination, the wet bias in the northern tropics is partly offset between these two components but the wet bias in the southern tropics is worsened (Fig. 1e). A very similar picture is found in CMIP5 (Fig. S1 in the online supplemental material). In the literature, both the symmetry index $(P_N + P_S)/2 - P_E$ (e.g., Samanta et al. 2019) and the asymmetry index $(P_N - P_S)/P_T$ (e.g., Hwang and Frierson 2013; Adam et al. 2016), where P_N, P_S, P_T, and P_E represent precipitation in the northern tropics, southern tropics, all tropics, and equator respectively, have been used to measure the severity of the double-ITCZ bias. The decomposition here indicates that each index only represents a part of the full double-ITCZ bias—respectively, the symmetric part that exists without the SST bias (AMIP − OBS) and the asymmetric part that arises from the SST bias (CMIP − AMIP).

The asymmetric tropical precipitation bias in CMIP − AMIP is a result of the asymmetric tropical SST bias. Tropical SST bias features a warm bias that is most pronounced in the southeastern oceans and cold bias that is most pronounced in the northwestern oceans (Fig. 1f). As illustrated in Xiang et al. (2017), tropical SST bias in CMIP (Fig. 1f) can be attributed to tropical CRE bias in AMIP (Fig. 1g). The spatial patterns of the SST bias in CMIP and the CRE bias in AMIP are broadly consistent, with warm (cold) bias inferred from the positive (negative) CRE bias at the top of the atmosphere (TOA; downward is positive). The positive (negative) CRE bias is more pronounced in the southern (northern) tropics (Fig. 1g), featuring a hemispherically asymmetric CRE bias that explains the asymmetric SST bias in CMIP (Fig. 1h). A decomposition of the TOA radiation flux shows that the shortwave CRE (SWCRE) is the dominating factor that contributes to the asymmetric radiation bias, while other factors such as the longwave CRE (LWCRE) and clear-sky radiation biases induce negligible hemispheric asymmetry (Fig. 1h). The pathway from the asymmetric CRE bias in AMIP to the asymmetric SST and precipitation biases arising after coupling (in CMIP − AMIP) is further supported by their correlations among individual models. The hemispheric asymmetry of tropical precipitation bias arising after coupling is correlated with the hemispheric asymmetry of tropical SST bias at $r = 0.78$ for CMIP5 and at $r = 0.89$ for CMIP6 (Fig. 1i). The hemispheric asymmetry of tropical precipitation bias is correlated with the hemispheric asymmetry of tropical SWCRE bias in atmospheric models at $r = 0.82$ for CMIP5 and $r = 0.72$ for CMIP6 (Fig. 1j).

Note that we do not expect the spatial patterns of the SST and precipitation bias in CMIP − AMIP and the CRE bias in AMIP to be exactly overlaid. The effect of tropical SST anomaly on precipitation is not just proportional to local SST anomaly but better understood as a shift in the climatological precipitation pattern (e.g., Zhou et al. 2019). The effect of CRE on SST can be advected by climatological ocean circulation and other processes such as atmospheric teleconnection between ocean basins can also modulate the spatial patterns of the SST bias (e.g., Wang et al. 2014; Zhou and Xie 2017a). Nevertheless, the hemispheric asymmetry of the SST and precipitation bias in CMIP − AMIP can be explained by the hemispheric asymmetry of the CRE bias in AMIP. Also, we emphasize that the CRE bias in AMIP cannot be a result of the SST bias because there is no SST bias in AMIP.

4. Hemispheric symmetry/asymmetry of tropical precipitation and CRE biases in atmospheric models determined by their dependency on climatological convective regime

The annual-mean precipitation and CRE biases in AMIP tend to be a function of the regimes of climatological convection (see definition of different convective regimes in section 2e). Specifically, the precipitation bias tends to be negative in the regime of strong convection but positive in the regime of moderate convection (Fig. 1b); the CRE bias tends to be positive in the

regime of stratocumulus, negative in the regime of moderate convection, and insignificant in the regime of strong convection (Fig. 1g).

Such dependencies of the precipitation and CRE biases on convective regimes are consistently seen throughout the seasonal cycle (Fig. 2). As tropical precipitation migrates north and south seasonally, the pattern of convection regimes shifts widely (Figs. 2a,b). In October, the convective region is mainly in the northern tropics and the nonconvective stratocumulus region is most pronounced in the southern tropics; in April, a substantial fraction of the convective region shifts to the southern tropics and the stratocumulus region becomes comparable between the two hemispheres. The precipitation and CRE biases closely follow such seasonal shift in the pattern of convection regimes, presenting invariant dependencies on convection regimes. In both months, the precipitation bias appears to be negative in the regime of strong convection and positive in the regime of moderate convection (Figs. 2c,d); the shortwave CRE bias appears to be negative in the regime of moderate convection and positive in the regimes of stratocumulus and strong convection (Figs. 2e,f); the longwave CRE bias appears to be negative in the regime of strong convection and insignificant in other regimes (Figs. 2g,h); in net, tropical CRE bias is negative in the regime of moderate convection, insignificant in the regime of strong convection, and positive in the stratocumulus regime (Figs. 2i,j).

The same dependencies are consistently seen in other months (February, May, August, and November), illustrating bias patterns that closely follow the seasonal shift of the climatological convective regimes (Fig. S2). Figure 3 further shows the probability distributions of the precipitation and CRE biases over different regimes for these four individual months. For each month, the distribution of the precipitation bias shows significant positive (negative) deviation from zero over the regime of moderate (strong) convection while the distributions of the CRE bias show significant positive (negative) deviation from zero over the regime of stratocumulus (moderate convection).

The dependencies of tropical precipitation and CRE biases in AMIP on convective regimes have direct consequences on their hemispheric asymmetries. For tropical precipitation bias, the wet bias in the regime of moderate convection is partially offset by the dry bias in the regime of strong convection in each hemisphere, so although the convective regions are more favored in the northern tropics, tropical precipitation bias in AMIP is nearly hemispherically symmetric (but slightly favors the northern tropics as shown by the orange line in Fig. 1e). For tropical CRE bias, because the bias is positive in the stratocumulus region that is favored in the dry hemisphere but negative or insignificant in the convective region that is favored in the wet hemisphere, it is deemed to input more energy into the dry hemisphere (i.e., to have a hemispheric asymmetry opposite to that of climatological tropical precipitation).

The connection from the dependency on convective regime to hemispheric asymmetry is further illustrated through the seasonal cycle. Figure 4 shows the monthly series of the

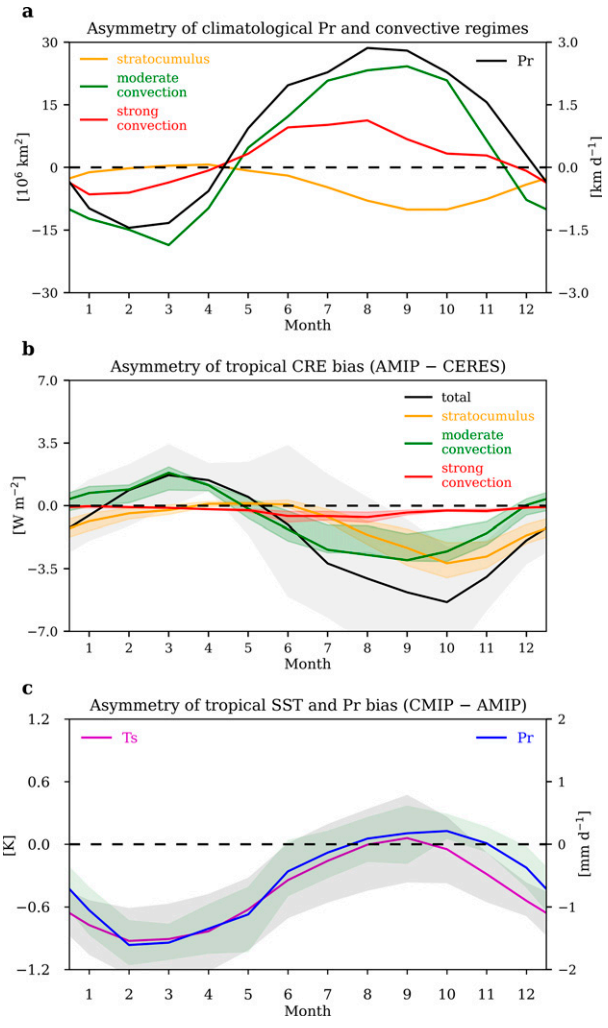

FIG. 4. (a) Monthly series of hemispheric asymmetry of tropical precipitation (black) and regime area of stratocumulus (yellow), moderate convection (green), and strong convection (red). Positive hemispheric asymmetry denotes larger values in the northern tropics. (b) Monthly series of hemispheric symmetry of tropical CRE bias in AMIP simulations (black) and the contributions from specific convective regimes (colored). (c) Monthly series of hemispheric symmetry of tropical biases in SST (magenta) and precipitation (blue) that arise after coupling to ocean (CMIP − AMIP). In (b) and (c), the line shows the model ensemble mean and the shading shows the range of the 25th and 75th percentiles of the model ensemble.

hemispheric asymmetry (defined as positive when the northern tropics are favored) of tropical precipitation, areas of different convective regimes, and the corresponding CRE bias. The stratocumulus (convective) region is most pronounced in the southern (northern) tropics when the northern tropics are in the rainy season. According to the monthly series, the hemispheric asymmetry of the area (defined as $A_{\mathrm{Asym}} = A_{0\text{–}30^\circ\mathrm{N}} - A_{0\text{–}30^\circ\mathrm{S}}$) of the stratocumulus (convective) regime is negatively (positively) correlated with the hemispheric asymmetry of tropical precipitation (Fig. 4a). Specifically, the correlations are 0.92 for strong

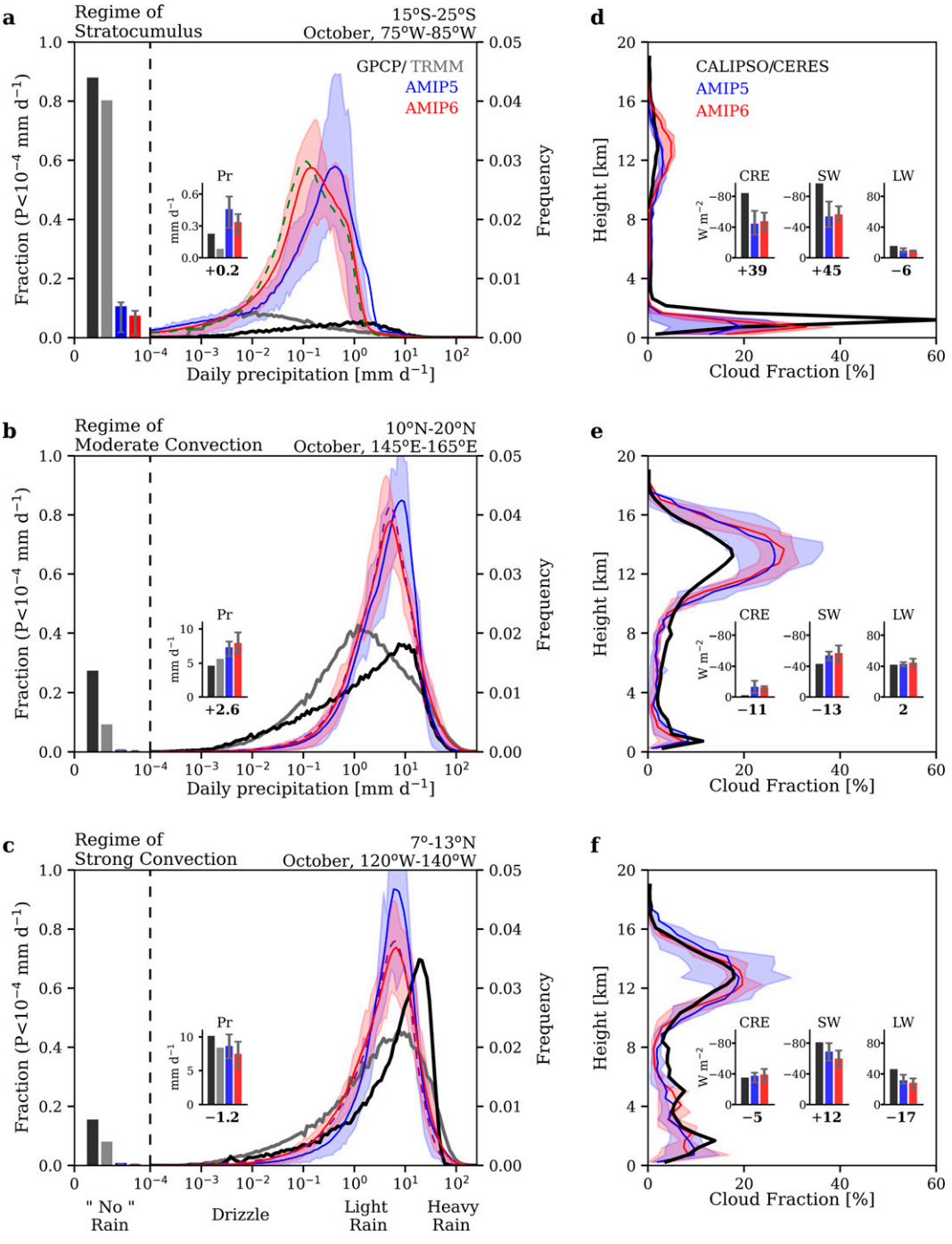

FIG. 5. (a)–(c) Distribution of daily precipitation intensity in GPCP (black), TRMM (gray), AMIP5 (blue; shading for the range of the 25th and 75th percentiles of the ensemble), and AMIP6 (red) over the representative region of the (a) stratocumulus, (b) moderate convection, and (c) strong convection regimes. The proportion of no-precipitation days is shown in the bar plot to the left. The mean precipitation in observations and models is shown in the bar plot to the right of the vertical dashed line, with the whiskers indicating the 25th and 75th percentiles of the model ensemble. The green dashed line in (a) indicates the distribution of resolved precipitation (from the cloud scheme) while the purple dashed lines in (b) and (c) indicate the distribution of convective precipitation (from the connective scheme). (d)–(f) Cloud fraction in *CALIPSO* and in AMIP5 and AMIP6 (from the *CALIPSO* simulator) over the representative region of the three convective regimes. The CRE (TOA; downward is positive), with its shortwave (SW) and longwave (LW) components, are shown in the bar plots. The ensemble-mean model biases are noted by the numbers below the *x* axis.

convection, 0.98 for moderate convection, and −0.81 for stratocumulus. As tropical CRE bias is positive (negative) over the stratocumulus (convective) regime, the hemispheric asymmetry of tropical CRE bias, in individual convective regimes and in total, is opposite to that of tropical precipitation and is most negative in late summer to early autumn (Fig. 4b). In the annual mean, as climatological tropical precipitation is asymmetrically favored in the northern tropics, the stratocumulus (convective) region is more pronounced in the southern (northern) tropics, so tropical CRE bias presents asymmetric energy input that favors the southern tropics. When atmospheric models are coupled to ocean, the hemispherically asymmetric CRE bias in atmospheric models further drives the hemispherically asymmetric SST and precipitation bias. The hemispheric asymmetry of tropical CRE bias is most negative in October while the hemispheric asymmetry of tropical SST bias is most negative in February (Fig. 4c). This delayed response reflects the effect of ocean heat capacity and potentially the effect of ocean circulation. The seasonal evolution of the hemispheric asymmetry of tropical precipitation bias closely follows that of tropical SST bias (Fig. 4c).

5. Mean precipitation and CRE biases in AMIP attributed to biases in local-scale precipitation characteristics

Finally, we show that the convective-regime-dependent biases in tropical precipitation and CRE in AMIP can be traced back to errors in representing local-scale precipitation characteristics (i.e., too frequent drizzling/convection). This is illustrated by comparing the distribution of the daily precipitation rate, the mean cloud profile, and the CRE in representative regions of the three convective regimes in both CMIP5 and CMIP6 models with observations (Fig. 5). Specifically, the stratocumulus regime is represented by tropical southeast Pacific Ocean (15°–25°S, 75°–85°W); the regime of moderate convection is represented by tropical northwest Pacific Ocean (10°–20°N, 145°–165°E); and the regime of strong convection is represented by the central region of the ITCZ (7°–13°N, 120°–140°W). These regions are noted by the blue rectangles in Fig. 2a.

In the regime of stratocumulus (Figs. 5a,d), precipitation is rare in observations. Among all the 1° × 1° daily grid data points from Octobers of 1979–2014, ~80% of them have no precipitation (identified as daily precipitation $P < 10^{-4}$ mm day^{-1}) and when it rains it is mostly drizzle ($10^{-4} < P < 1$ mm day^{-1}). This large proportion of no-precipitation days is substantially underestimated by GCMs (in which only ~10% of days have no precipitation) and the occurrence of drizzle is substantially overestimated. The overly active drizzling is mainly contributed by grid-resolved precipitation from the cloud scheme (green dashed line in Fig. 5a), as convective parameterization is largely inactive in the stratocumulus regime. The too-frequent drizzling, along with substantially underestimated no-precipitation occurrence, results in a positive bias in the mean precipitation. The too-frequent drizzling corresponds to reduced occurrence of stratocumulus and consequently a substantial negative bias in the amount of low-level clouds. There is also a slight positive

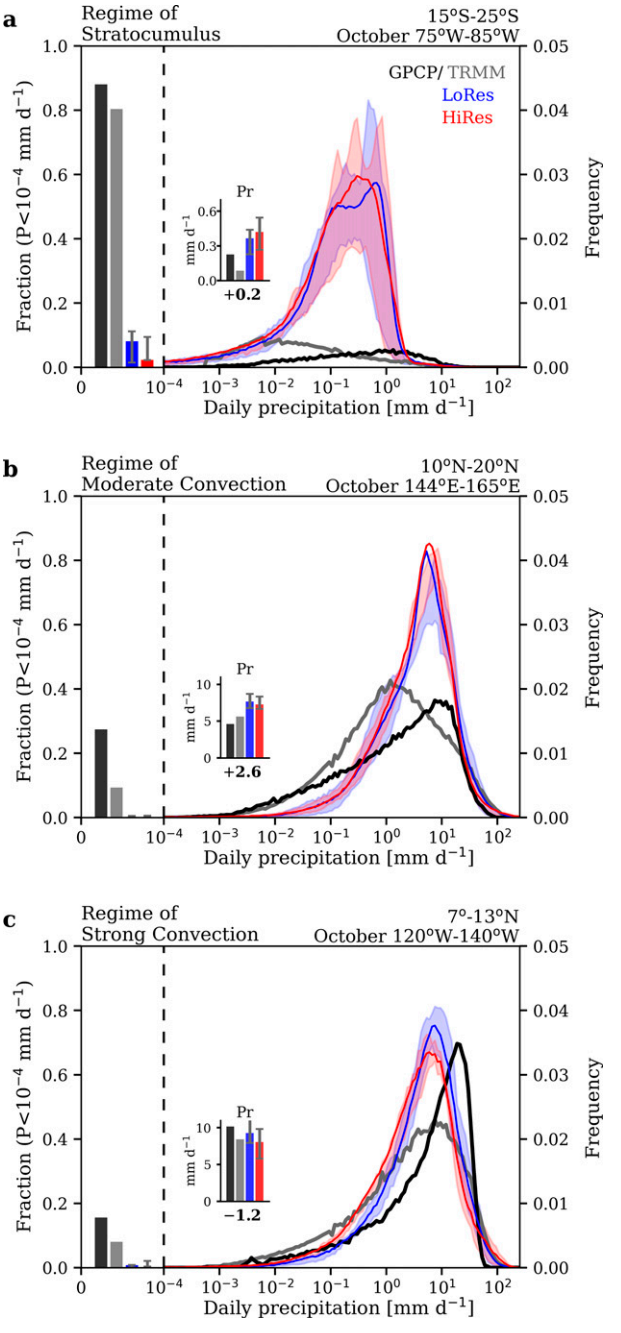

FIG. 6. Distribution of daily precipitation intensity in GPCP (black), TRMM (gray), LoRes (blue; shading for the range of the 25th and 75th percentiles of the ensemble), and HiRes (red) over the representative region of the (a) stratocumulus, (b) moderate convection, and (c) strong convection regimes. The proportion of no-precipitation days is shown in the bar plot to the left. The mean precipitation in observations and models is shown in the bar plot to the right of the dashed line, with the mean model bias noted below the *x* axis.

bias in the high-level clouds, suggesting too frequent transitions from stratocumulus to cumulus in models. Dominated by the negative bias in the low-level clouds, the negative SWCRE is substantially underestimated by models. The LWCRE bias is

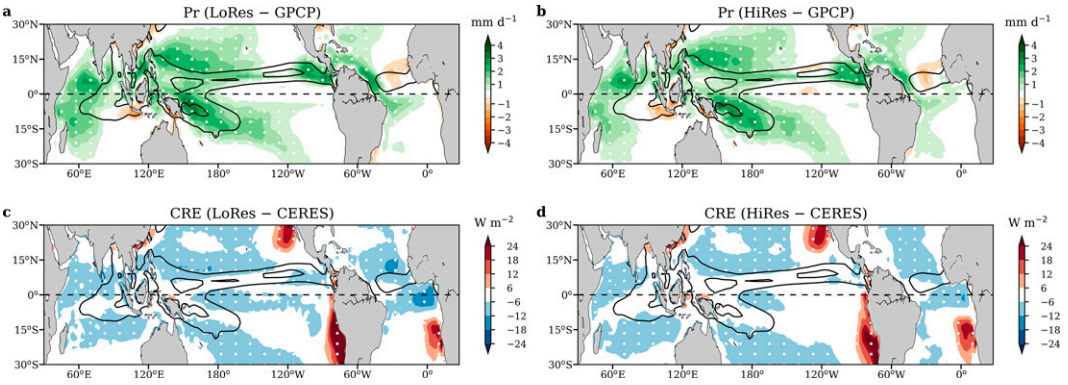

FIG. 7. Spatial pattern of annual-mean tropical precipitation and CRE biases in (a),(c) LoRes and (b),(d) HiRes.

less significant, so the net CRE bias is positive in the regime of stratocumulus.

In the regime of moderate convection (Figs. 5b,e), observed daily precipitation is dominated by light rain ($1 < P <$ 10 mm day^{-1}). In GCMs, the frequency of no precipitation or drizzle ($P < 1$ mm day^{-1}) is underestimated while the frequency of light rain is overestimated ($1 < P < 10$ mm day^{-1}). As precipitation is dominated by convective precipitation in this regime, the above bias is mainly contributed by convective precipitation (purple dashed line in Fig. 5b). As the overly active convection shifts daily precipitation from drizzle to light rain, there is a positive bias in the mean precipitation. The total cloud fraction increases correspondingly, leading to a more negative SWCRE. The LWCRE bias is insignificant so the net CRE bias is negative in the regime of moderate convection.

In the regime of strong convection (Figs. 5c,f), observed daily precipitation is dominated by heavy precipitation ($P > 20$ mm day^{-1}). In GCMs, however, the occurrence of heavy rain is underestimated and the occurrence of light rain is overestimated. Such bias is again consistent with the overly active convection, which releases convective instability too often and suppresses the formation of intense events. As heavy precipitation dominates the mean precipitation in this regime of strong convection, the suppression of heavy precipitation leads to a negative bias in the mean precipitation. Correspondingly, the mean height of the high-level cloud and the amount of the midlevel cloud are reduced in models compared to *CALIPSO*. As a result of the reduced amount of midlevel cloud, the negative SWCRE is underestimated by models; due to the lower height of high-level cloud, the positive LWCRE is underestimated. In net, there is slightly negative but insignificant CRE bias in the regime of strong convection.

We note that there are notable differences in daily precipitation characteristics among different observation datasets. For example, the precipitation rate of peak occurrence over a specific convective regime can be an order of magnitude apart between GPCP and TRMM. Such difference indicates current uncertainty in precipitation measurements. Nevertheless, the differences between models and observations are more substantial than the differences among observations. Besides the GPCP and TRMM datasets, we have compared the model simulations with two other precipitation datasets, CMORPH and PERSIANN-CDR. The bias of too frequent drizzling/convection and its impacts on the mean precipitation as a function of convective regimes are robustly present (Fig. S3).

The convective-regime-dependent effects of too frequent drizzling/convection on the mean precipitation and CRE are consistently present in other representative regions of these three convective regimes (Figs. S4–S6). The convective-regime-dependent precipitation bias directly corresponds to the hemispherically symmetric wet bias in atmospheric models. The convective-regime-dependent CRE biases in atmospheric models are deemed to favor the southern tropics and drive the hemispherically asymmetric biases of SST and precipitation when atmospheric models are coupled to ocean. Through such direct and SST-mediated pathways, the local-scale characteristic bias of too frequent drizzling/convection leads to the large-scale double-ITCZ bias.

6. Consistent local- and large-scale precipitation bias in high-resolution models

The subgrid parameterizations of unresolved physical processes have long been blamed for misrepresentation of atmospheric convection and biases in tropical precipitation pattern. It is believed that increasing horizontal resolution would improve the model simulation by reducing the dependency on subgrid parameterization (e.g., convective parameterization), better representing the boundary condition (e.g., topography), and better resolving dynamic processes (e.g., mesoscale convective systems and storms). Here, potential benefits of higher resolution are investigated using model outputs from the HighResMIP and DYAMOND projects. The HighResMIP project provides paired AMIP-style simulations with both standard (1°–2°) and enhanced (0.25°–0.5°) horizontal resolutions. The DYAMOND project uses nonhydrostatic atmospheric models with storm-resolving resolutions (a few kilometers).

The intensity distribution and large-scale pattern of tropical precipitation are compared between the simulations with enhanced (referred to as HiRes) and standard (referred to as LoRes) horizontal resolutions in HighResMIP

(Fig. 6). We find that mesoscale horizontal resolution does not alleviate the local- and large-scale precipitation biases. The local-scale bias of too frequent drizzling/convection is consistently present in both LoRes and HiRes simulations. In the stratocumulus regime, the frequency of no precipitation is substantially underestimated and the frequency of drizzling is overestimated; in the regime of moderate convection, the frequency of drizzling or no precipitation is underestimated and that of light rain is overestimated; and in the regime of strong convection, the frequency of no or heavy precipitation is underestimated and that of light rain is overestimated. Along with local-scale drizzling bias, HiRes presents the same large-scale pattern bias in tropical precipitation and CRE as LoRes (Fig. 7). The precipitation bias features wet biases over the moderate convective region and dry or insignificant biases in the regime of strong convection. The CRE bias features positive bias over the regime of stratocumulus, negative bias over the regime of moderate convection, and insignificant bias over the regime of strong convection. In the HighResMIP models with enhanced resolution of 0.25°–0.5°, many aspects of the simulations such as tropical cyclones are improved (Balaguru et al. 2020; Roberts et al. 2020). However, shallow and deep convection are still subgrid features and need to be parameterized. It is thus not surprising that the precipitation biases, in both local-scale characteristics and large-scale pattern, remain nearly unchanged.

Next, the intensity distribution and large-scale pattern of tropical precipitation are investigated in the DYAMOND models (Fig. 8). Our analysis suggests that while the frequency of heavy precipitation is better simulated with the storm-resolving resolution, the drizzling and double-ITCZ biases of tropical precipitation remain. The local-scale bias is still notable with reduced occurrence of no-precipitation days and increased occurrence of light rain relative to observations. For large-scale precipitation pattern, the difference between individual models and observations is twice as large as the climatological bias in the AMIP models (Fig. S7). For a single 30-day period, atmospheric internal variability would induce substantial differences between individual models and observations. The effect of atmospheric internal dynamics should be partially offset in the five-model ensemble mean, which suggests a precipitation bias pattern that is broadly similar to that of AMIP, featuring dry bias in the strong convective region and wet bias in the surrounding moderate convective region (Fig. 9). While the storm-resolving resolution removes the need to parameterize deep convection, shallow convection and boundary layer turbulence remain subgrid features. In some DYAMOND models no parameterization of shallow convection is used while in others shallow convection parameterization similar to that in CMIP models is used (Table 3). It is thus not unexpected that the local-scale bias of too frequent drizzling/convection is still present in the DYAMOND models. Previous studies have also shown that the DYAMOND models do not significantly improve the representation of marine boundary layer clouds (Heim et al. 2021).

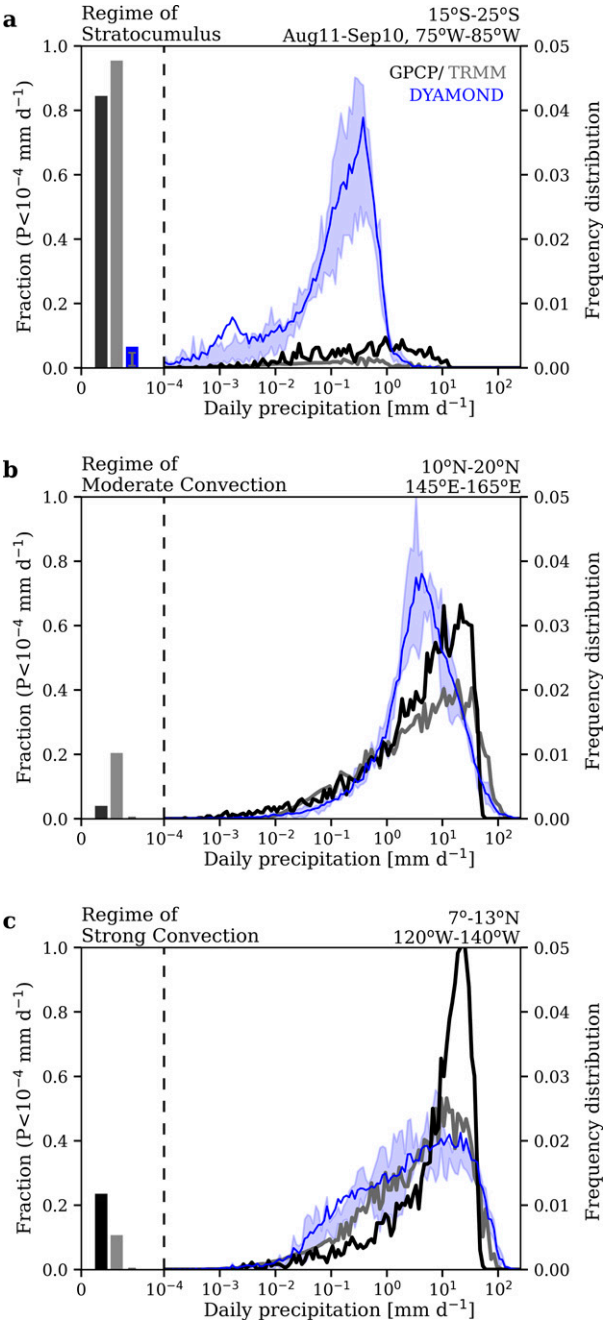

FIG. 8. Distribution of daily precipitation intensity in GPCP (black), TRMM (gray), and DYAMOND (blue line and shading for the mean and the range of the 25th and 75th percentiles of the ensemble) over the representative region of the (a) stratocumulus and the (b) moderate and (c) strong convection regimes. The proportion of no-precipitation days is shown in the bar plot to the left.

7. Summary and discussion

By analyzing biases of precipitation, cloud, and radiation in both atmospheric and coupled models, our study establishes a physical linkage from the local-scale characteristic bias of too frequent drizzling/convection to the large-scale pattern bias

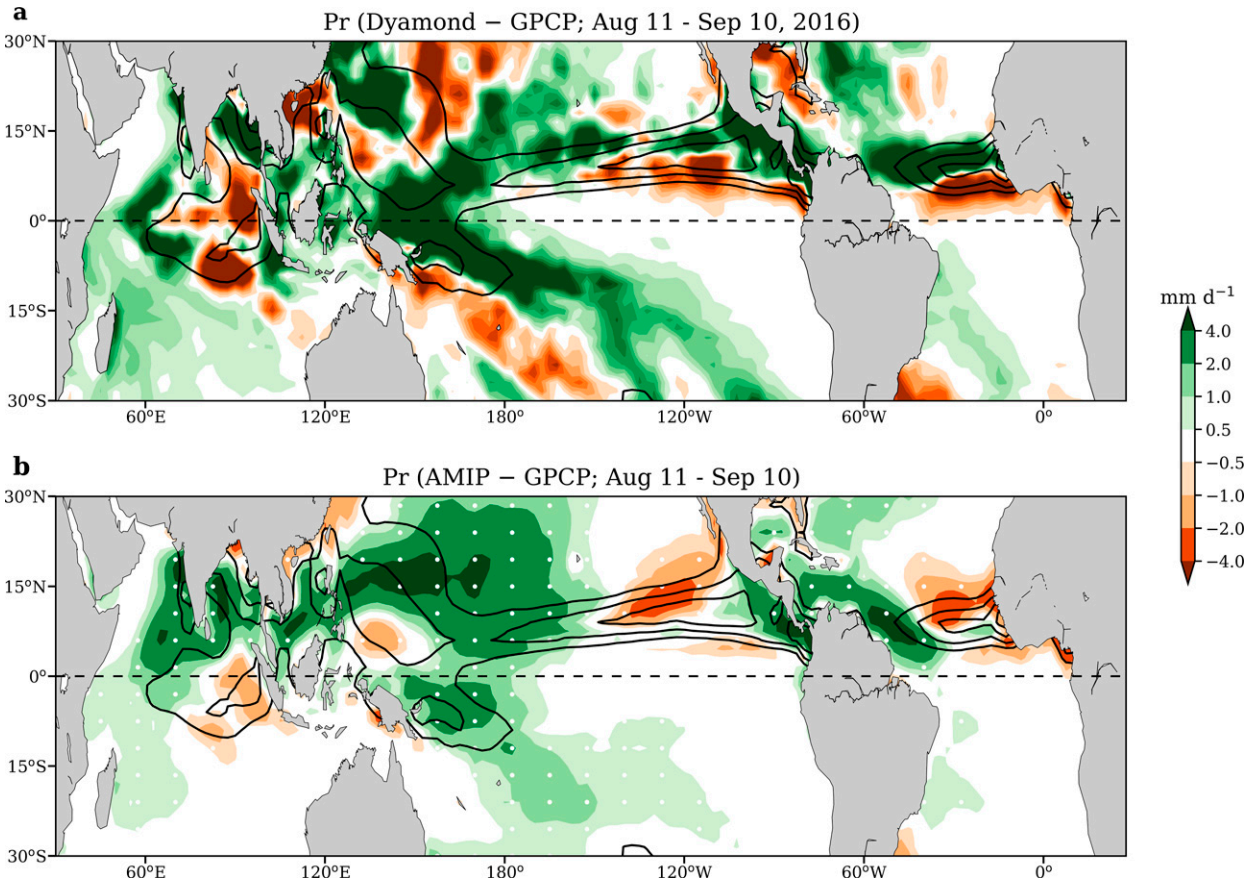

FIG. 9. (a) Tropical precipitation difference between DYAMOND and GPCP over the period 11 Aug–10 Sep 2016. (b) Climatological tropical precipitation bias in AMIP for the period 11 Aug–10 Sep.

of double ITCZ. The physical linkage through both direct and indirect pathways is schematically illustrated in Fig. 10 (following the order of sections 6 → 5 → 4 → 3). Directly, local-scale drizzling bias contributes to the hemispherically symmetric wet bias in atmospheric models without SST biases, by increasing light precipitation in the regime of moderate convection and suppressing heavy precipitation in the regime of strong convection (yellow pathway in Fig. 10). Indirectly, a local-scale drizzling bias drives the hemispherically asymmetric precipitation bias in coupled simulations through its influences on the CRE and consequently SST (blue pathway in Fig. 10). Specifically, too frequent drizzling/convection induces positive CRE bias in the stratocumulus region (by breaking the sunlight-reflecting low-level clouds), negative CRE bias in the moderate convective region (by increasing total cloud amount and enhancing negative SWCRE in the regime of moderate convection), and insignificant CRE bias in the regime of strong convection. Such dependency on convective regime leads to more positive CRE bias in the southern tropics as the stratocumulus (convective) region is more pronounced in the southern (northern) tropics. The hemispherically asymmetric CRE bias then drives warm and wet (cool and dry) biases in the southern (northern) tropics when atmospheric models are coupled to ocean. Together, the direct and indirect effects lead to the full double-ITCZ bias in coupled models. Our results thus connect the two outstanding model biases at local and large scale, and suggest correcting the local-scale characteristic bias of too frequent drizzling/convection as a critical step for fixing the large-scale double-ITCZ bias.

There are more than 20 climate models participating in CMIP6. They are developed by various modeling centers around the world, with different designs of physical parameterizations and dynamical cores. Yet, these models share the same drizzling and double-ITCZ biases (along with the similar pattern of tropical SST and CRE bias) and there is no significant improvement in these biases despite generations of model development. Such persistent and common biases are likely due to some shared limitations in subgrid parameterizations (e.g., convection, boundary layer, clouds, microphysics), and/or the physics–dynamics coupling (Gross et al. 2018), and/or limitations in the concept of decomposition of the simulation of fluid dynamics into resolved grid-mean circulation and parameterized subgrid processes. It has been shown that tuning convective schemes (e.g., Oueslati and Bellon 2013; Song and Zhang 2018) or modifying the topography (e.g., Baldwin et al. 2021) can improve the simulation of tropical precipitation. However, these improvements are often regional and small in magnitude to effectively eliminate the double-ITCZ bias.

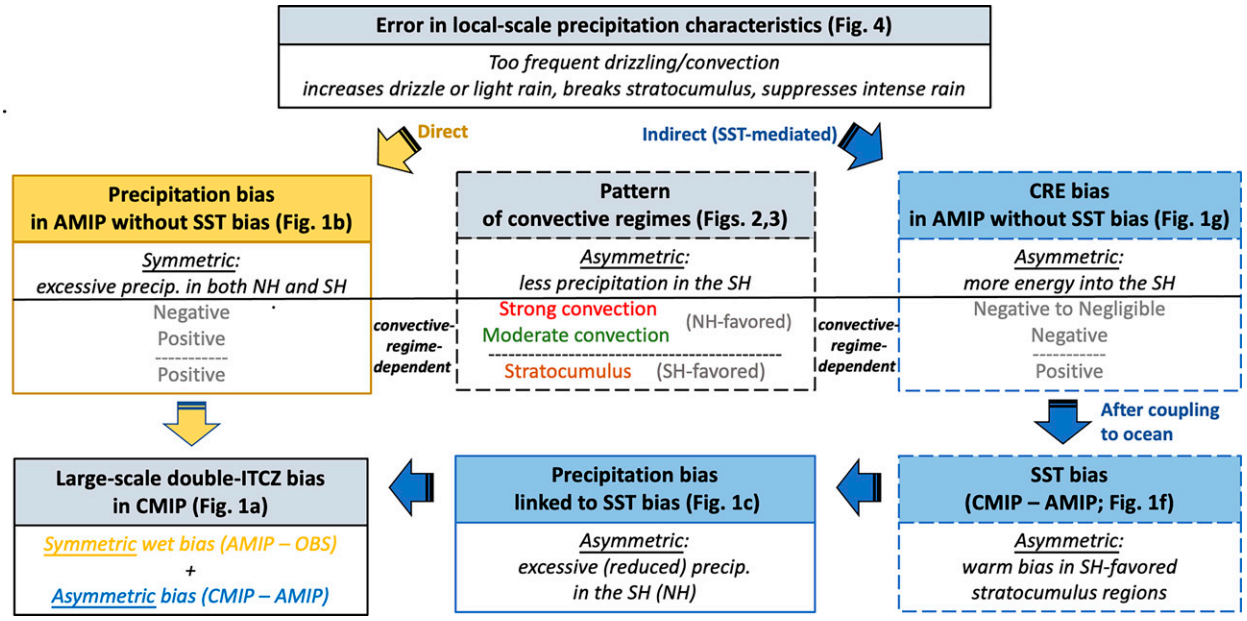

FIG. 10. The physical linkage from local-scale bias of too frequent drizzling/convection to large-scale double-ITCZ bias through direct (existing without SST biases; yellow arrows) and indirect (SST-mediated; blue arrows) pathways.

The slow progress in low-resolution (1°–2°) climate modeling with intensive subgrid parameterizations has motivated high-resolution modeling that less depends on subgrid parameterizations. However, our results show that the precipitation biases are not alleviated in models with mesoscale (HighResMIP) and even storm-resolving (DYAMOND) resolution. This suggests that subgrid parameterizations of small-scale processes such as boundary layer mixing and cloud formation (micro- and macrophysics) may be largely responsible for tropical precipitation biases, as such processes are still parameterized in high-resolution and storm-resolving models. For example, a stratocumulus cloud and the associated cloud-top entrainment, inversion, and radiative cooling occur in a very thin vertical layer. It is a major challenge for boundary schemes to satisfactorily simulate such small-scale processes. Also, current climate models often use separated subgrid schemes to parameterize the closely coupled boundary layer and convection; such artificial separation may lead to inconsistency and errors. Furthermore, precipitation formation is sensitive to microphysics processes (e.g., Qian et al. 2009) and biases in microphysics parameterization may contribute to the drizzling bias. While further refining subgrid parameterizations may help, models with large-eddy resolution (~100 m) or ultraparameterization (Parishani et al. 2017) would be valuable for understanding and correcting tropical precipitation biases. Last, machine learning offers new opportunities to improve subgrid parameterizations and model tuning (e.g., Chantry et al. 2021), and using metrics that target their ability to reduce biases in the training should be valuable.

Acknowledgments. This study was supported by Office of Science, U.S. Department of Energy Biological and Environmental Research as part of the Regional and Global Model Analysis program area. We acknowledge the WCRP Working Group on Coupled Modeling, which is responsible for the CMIP. The Pacific Northwest National Laboratory (PNNL) is operated for DOE by Battelle Memorial Institute under contract DE-AC05-76RLO1830. The authors declare that they have no competing interests. DYAMOND data management was provided by the German Climate Computing Center (DKRZ) and supported through the projects ESiWACE and ESiWACE2. The projects ESiWACE and ESiWACE2 have received funding from the European Union's Horizon 2020 research and innovation programme under grant agreements 675191 and 823988. This work used resources of the Deutsches Klimarechenzentrum (DKRZ) granted by its Scientific Steering Committee (WLA) under project IDs bk1040 and bb1153.

Data availability statement. The HadISST dataset is available at https://www.metoffice.gov.uk/hadobs/hadisst. The GPCP and CMAP precipitation datasets are available at https://psl.noaa.gov/data/gridded/data.gpcp.html and https://psl.noaa.gov/data/gridded/data.cmap.html, respectively. The CERES radiation dataset is available at https://ceres.larc.nasa.gov/data/. The CALIPSO cloud fraction dataset is available at https://climserv.ipsl.polytechnique.fr/cfmip-obs/Calipso_goccp.html. The DYAMOND dataset is available upon request at https://www.esiwace.eu/services/dyamond-initiative/services-dyamond-summer.

REFERENCES

Adam, O., T. Schneider, F. Brient, and T. Bischoff, 2016: Relation of the double-ITCZ bias to the atmospheric energy budget in climate models. *Geophys. Res. Lett.*, **43**, 7670–7677, https://doi.org/10.1002/2016GL069465.

——, ——, and ——, 2018: Regional and seasonal variations of the double-ITCZ bias in CMIP5 models. *Climate Dyn.*, **51**, 101–117, https://doi.org/10.1007/s00382-017-3909-1.

Adler, R. F., and Coauthors, 2018: The Global Precipitation Climatology Project (GPCP) monthly analysis (new version 2.3) and a review of 2017 global precipitation. *Atmosphere*, **9**, 138, https://doi.org/10.3390/atmos9040138.

Ashouri, H., K.-L. Hsu, S. Sorooshian, D. K. Braithwaite, K. R. Knapp, L. D. Cecil, B. R. Nelson, and O. P. Prat, 2015: PERSIANN-CDR: Daily precipitation climate data record from multisatellite observations for hydrological and climate studies. *Bull. Amer. Meteor. Soc.*, **96**, 69–83, https://doi.org/10.1175/BAMS-D-13-00068.1.

Balaguru, K., and Coauthors, 2020: Characterizing tropical cyclones in the Energy Exascale Earth System model version 1. *J. Adv. Model. Earth Syst.*, **12**, e2019MS002024, https://doi.org/10.1029/2019MS002024.

Baldwin, J. W., A. R. Atwood, G. A. Vecchi, and D. S. Battisti, 2021: Outsize influence of Central American orography on global climate. *AGU Adv.*, **2**, e2020AV000343, https://doi.org/10.1029/2020AV000343.

Bodas-Salcedo, A., and Coauthors, 2011: COSP: Satellite simulation software for model assessment. *Bull. Amer. Meteor. Soc.*, **92**, 1023–1043, https://doi.org/10.1175/2011BAMS2856.1.

Chantry, M., H. Christensen, P. Dueben, and T. Palmer, 2021: Opportunities and challenges for machine learning in weather and climate modelling: Hard, medium and soft AI. *Philos. Trans. Roy. Soc.*, **A379**, 20200083, https://doi.org/10.1098/rsta.2020.0083.

Chepfer, H., S. Bony, D. Winker, G. Cesana, J. L. Dufresne, P. Minnis, C. J. Stubenrauch, and S. Zeng, 2010: The GCM-Oriented CALIPSO Cloud Product (CALIPSO-GOCCP). *J. Geophys. Res.*, **115**, D00H16, https://doi.org/10.1029/2009JD012251.

Dai, A., 2006: Precipitation characteristics in eighteen coupled climate models. *J. Climate*, **19**, 4605–4630, https://doi.org/10.1175/JCLI3884.1.

de Szoeke, S. P., and S.-P. Xie, 2008: The tropical eastern Pacific seasonal cycle: Assessment of errors and mechanisms in IPCC AR4 coupled ocean–atmosphere general circulation models. *J. Climate*, **21**, 2573–2590, https://doi.org/10.1175/2007JCLI1975.1.

Dong, L., L. R. Leung, J. Lu, and F. Song, 2021: Double-ITCZ as an emergent constraint for future precipitation over Mediterranean climate regions in the North Hemisphere. *Geophys. Res. Lett.*, **48**, e2020GL091569, https://doi.org/10.1029/2020GL091569.

Eyring, V., S. Bony, G. A. Meehl, C. A. Senior, B. Stevens, R. J. Stouffer, and K. E. Taylor, 2016: Overview of the Coupled Model Intercomparison Project Phase 6 (CMIP6) experimental design and organization. *Geosci. Model Dev.*, **9**, 1937–1958, https://doi.org/10.5194/gmd-9-1937-2016.

Fiedler, S., and Coauthors, 2020: Simulated tropical precipitation assessed across three major phases of the Coupled Model Intercomparison Project (CMIP). *Mon. Wea. Rev.*, **148**, 3653–3680, https://doi.org/10.1175/MWR-D-19-0404.1.

Grant, A. L. M., 2001: Cloud-base fluxes in the cumulus-capped boundary layer. *Quart. J. Roy. Meteor. Soc.*, **127**, 407–421, https://doi.org/10.1002/qj.49712757209.

Gross, M., and Coauthors, 2018: Physics–dynamics coupling in weather, climate, and Earth system models: Challenges and recent progress. *Mon. Wea. Rev.*, **146**, 3505–3544, https://doi.org/10.1175/MWR-D-17-0345.1.

Haarsma, R. J., and Coauthors, 2016: High Resolution Model Intercomparison Project (HighResMIP v1.0) for CMIP6. *Geosci. Model Dev.*, **9**, 4185–4208, https://doi.org/10.5194/gmd-9-4185-2016.

Hawcroft, M., J. M. Haywood, M. Collins, A. Jones, A. C. Jones, and G. Stephens, 2017: Southern Ocean albedo, inter-hemispheric energy transports and the double ITCZ: Global impacts of biases in a coupled model. *Climate Dyn.*, **48**, 2279–2295, https://doi.org/10.1007/s00382-016-3205-5.

Heim, C., L. Hentgen, N. Ban, and C. Schär, 2021: Inter-model variability in convection-resolving simulations of subtropical marine low clouds. *J. Meteor. Soc. Japan*, **99**, 1271–1295, https://doi.org/10.2151/jmsj.2021-062.

Huffman, G. J., and Coauthors, 2007: The TRMM Multisatellite Precipitation Analysis (TMPA): Quasi-global, multiyear, combined-sensor precipitation estimates at fine scales. *J. Hydrometeor.*, **8**, 38–55, https://doi.org/10.1175/JHM560.1.

Hwang, Y.-T., and D. M. W. Frierson, 2013: Link between the double-Intertropical Convergence Zone problem and cloud biases over the Southern Ocean. *Proc. Natl. Acad. Sci. USA*, **110**, 4935–4940, https://doi.org/10.1073/pnas.1213302110.

Joyce, R. J., J. E. Janowiak, P. A. Arkin, and P. Xie, 2004: CMORPH: A method that produces global precipitation estimates from passive microwave and infrared data at high spatial and temporal resolution. *J. Hydrometeor.*, **5**, 487–503, https://doi.org/10.1175/1525-7541(2004)005<0487:CAMTPG>2.0.CO;2.

Kang, S. M., I. M. Held, D. M. W. Frierson, and M. Zhao, 2008: The response of the ITCZ to extratropical thermal forcing: Idealized slab-ocean experiments with a GCM. *J. Climate*, **21**, 3521–3532, https://doi.org/10.1175/2007JCLI2146.1.

Kay, J. E., and Coauthors, 2012: Exposing global cloud biases in the Community Atmosphere Model (CAM) using satellite observations and their corresponding instrument simulators. *J. Climate*, **25**, 5190–5207, https://doi.org/10.1175/JCLI-D-11-00469.1.

Khairoutdinov, M. F., P. N. Blossey, and C. S. Bretherton, 2022: Global system for atmospheric modeling: Model description and preliminary results. *J. Adv. Model. Earth Syst.*, **14**, e2021MS002968, https://doi.org/10.1029/2021MS002968.

Li, G., and S.-P. Xie, 2014: Tropical biases in CMIP5 multimodel ensemble: The excessive equatorial Pacific cold tongue and double ITCZ problems. *J. Climate*, **27**, 1765–1780, https://doi.org/10.1175/JCLI-D-13-00337.1.

Lin, J.-L., 2007: The double-ITCZ problem in IPCC AR4 coupled GCMs: Ocean–atmosphere feedback analysis. *J. Climate*, **20**, 4497–4525, https://doi.org/10.1175/JCLI4272.1.

Lin, S.-J., 2004: A "vertically Lagrangian" finite-volume dynamical core for global models. *Mon. Wea. Rev.*, **132**, 2293–2307, https://doi.org/10.1175/1520-0493(2004)132<2293:AVLFDC>2.0.CO;2.

Ma, C.-C., C. R. Mechoso, A. W. Robertson, and A. Arakawa, 1996: Peruvian stratus clouds and the tropical Pacific circulation: A coupled ocean–atmosphere GCM study. *J. Climate*, **9**, 1635–1645, https://doi.org/10.1175/1520-0442(1996)009<1635:PSCATT>2.0.CO;2.

Mechoso, C. R., and Coauthors, 1995: The seasonal cycle over the tropical Pacific in coupled ocean–atmosphere general circulation models. *Mon. Wea. Rev.*, **123**, 2825–2838, https://doi.org/10.1175/1520-0493(1995)123<2825:TSCOTT>2.0.CO;2.

Nam, C., S. Bony, J.-L. Dufresne, and H. Chepfer, 2012: The 'too few, too bright' tropical low-cloud problem in CMIP5

models. *Geophys. Res. Lett.*, **39**, L21801, https://doi.org/10.1029/2012GL053421.

Oueslati, B., and G. Bellon, 2013: Convective entrainment and large-scale organization of tropical precipitation: Sensitivity of the CNRM-CM5 hierarchy of models. *J. Climate*, **26**, 2931–2946, https://doi.org/10.1175/JCLI-D-12-00314.1.

Parishani, H., M. S. Pritchard, C. S. Bretherton, M. C. Wyant, and M. Khairoutdinov, 2017: Toward low-cloud-permitting cloud superparameterization with explicit boundary layer turbulence. *J. Adv. Model. Earth Syst.*, **9**, 1542–1571, https://doi.org/10.1002/2017MS000968.

Putman, W. M., and M. Suarez, 2011: Cloud-system resolving simulations with the NASA Goddard Earth Observing System global atmospheric model (GEOS-5). *Geophys. Res. Lett.*, **38**, https://doi.org/10.1029/2011GL048438.

Qian, Y., D. Gong, J. Fan, L. R. Leung, R. Bennartz, D. Chen, and W. Wang, 2009: Heavy pollution suppresses light rain in China: Observations and modeling. *J. Geophys. Res.*, **114**, D00K02, https://doi.org/10.1029/2008JD011575.

Rayner, N. A., D. E. Parker, E. B. Horton, C. K. Folland, L. V. Alexander, D. P. Rowell, E. C. Kent, and A. Kaplan, 2003: Global analyses of sea surface temperature, sea ice, and night marine air temperature since the late nineteenth century. *J. Geophys. Res.*, **108**, 4407, https://doi.org/10.1029/2002JD002670.

Roberts, M. J., and Coauthors, 2020: Impact of model resolution on tropical cyclone simulation using the HighResMIP–PRIMAVERA multimodel ensemble. *J. Climate*, **33**, 2557–2583, https://doi.org/10.1175/JCLI-D-19-0639.1.

Samanta, D., K. B. Karnauskas, and N. F. Goodkin, 2019: Tropical Pacific SST and ITCZ biases in climate models: Double trouble for future rainfall projections? *Geophys. Res. Lett.*, **46**, 2242–2252, https://doi.org/10.1029/2018GL081363.

Satoh, M., and Coauthors, 2014: The Non-hydrostatic Icosahedral Atmospheric Model: Description and development. *Prog. Earth Planet. Sci.*, **1**, 18, https://doi.org/10.1186/s40645-014-0018-1.

Song, X., and G. J. Zhang, 2018: The roles of convection parameterization in the formation of double ITCZ syndrome in the NCAR CESM: I. Atmospheric processes. *J. Adv. Model. Earth Syst.*, **10**, 842–866, https://doi.org/10.1002/2017MS001191.

Stephens, G. L., and Coauthors, 2010: Dreary state of precipitation in global models. *J. Geophys. Res.*, **115**, D24211, https://doi.org/10.1029/2010JD014532.

Stevens, B., and Coauthors, 2019: DYAMOND: The DYnamics of the Atmospheric general circulation Modeled On Non-hydrostatic Domains. *Prog. Earth Planet. Sci.*, **6**, 61, https://doi.org/10.1186/s40645-019-0304-z.

Taylor, K. E., R. J. Stouffer, and G. A. Meehl, 2011: An overview of CMIP5 and the experiment design. *Bull. Amer. Meteor. Soc.*, **93**, 485–498, https://doi.org/10.1175/BAMS-D-11-00094.1.

Tian, B., and X. Dong, 2020: The double-ITCZ bias in CMIP3, CMIP5, and CMIP6 models based on annual mean precipitation. *Geophys. Res. Lett.*, **47**, e2020GL087232, https://doi.org/10.1029/2020GL087232.

Tomas, R. A., C. Deser, and L. Sun, 2016: The role of ocean heat transport in the global climate response to projected Arctic sea ice loss. *J. Climate*, **29**, 6841–6859, https://doi.org/10.1175/JCLI-D-15-0651.1.

Trenberth, K. E., and J. T. Fasullo, 2010: Simulation of present-day and twenty-first-century energy budgets of the southern oceans. *J. Climate*, **23**, 440–454, https://doi.org/10.1175/2009JCLI3152.1.

——, and Y. Zhang, 2018: How often does it really rain? *Bull. Amer. Meteor. Soc.*, **99**, 289–298, https://doi.org/10.1175/BAMS-D-17-0107.1.

Walters, D., and Coauthors, 2019: The Met Office Unified Model Global Atmosphere 7.0/7.1 and JULES Global Land 7.0 configurations. *Geosci. Model Dev.*, **12**, 1909–1963, https://doi.org/10.5194/gmd-12-1909-2019.

Wang, C., L. Zhang, S.-K. Lee, L. Wu, and C. R. Mechoso, 2014: A global perspective on CMIP5 climate model biases. *Nat. Climate Change*, **4**, 201–205, https://doi.org/10.1038/nclimate2118.

Wielicki, B. A., B. R. Barkstrom, E. F. Harrison, R. B. Lee, G. L. Smith, and J. E. Cooper, 1996: Clouds and the Earth's Radiant Energy System (CERES): An Earth observing system experiment. *Bull. Amer. Meteor. Soc.*, **77**, 853–868, https://doi.org/10.1175/1520-0477(1996)077<0853:CATERE>2.0.CO;2.

Wood, N., and Coauthors, 2014: An inherently mass-conserving semi-implicit semi-Lagrangian discretization of the deep-atmosphere global non-hydrostatic equations. *Quart. J. Roy. Meteor. Soc.*, **140**, 1505–1520, https://doi.org/10.1002/qj.2235.

Xiang, B., M. Zhao, I. M. Held, and J.-C. Golaz, 2017: Predicting the severity of spurious "double ITCZ" problem in CMIP5 coupled models from AMIP simulations. *Geophys. Res. Lett.*, **44**, 1520–1527, https://doi.org/10.1002/2016GL071992.

——, ——, Y. Ming, W. Yu, and S. M. Kang, 2018: Contrasting impacts of radiative forcing in the Southern Ocean versus southern tropics on ITCZ position and energy transport in one GFDL climate model. *J. Climate*, **31**, 5609–5628, https://doi.org/10.1175/JCLI-D-17-0566.1.

Zhang, M. H., and Coauthors, 2005: Comparing clouds and their seasonal variations in 10 atmospheric general circulation models with satellite measurements. *J. Geophys. Res.*, **110**, D15S02, https://doi.org/10.1029/2004JD005021.

Zhou, W., and S.-P. Xie, 2017a: Intermodel spread around the Kuroshio–Oyashio Extension region in coupled GCMs caused by meridional variation of the westerly jet from atmospheric GCMs. *J. Climate*, **30**, 4589–4599, https://doi.org/10.1175/JCLI-D-16-0831.1.

——, and ——, 2017b: Intermodel spread of the double-ITCZ bias in coupled GCMs tied to land surface temperature in AMIP GCMs. *Geophys. Res. Lett.*, **44**, 7975–7984, https://doi.org/10.1002/2017GL074377.

——, ——, and D. Yang, 2019: Enhanced equatorial warming causes deep-tropical contraction and subtropical monsoon shift. *Nat. Climate Change*, **9**, 834–839, https://doi.org/10.1038/s41558-019-0603-9.

Zhou, Z.-Q., and S.-P. Xie, 2015: Effects of climatological model biases on the projection of tropical climate change. *J. Climate*, **28**, 9909–9917, https://doi.org/10.1175/JCLI-D-15-0243.1.